New Journal of Physics
The open access journal at the forefront of physics

Deutsche Physikalische Gesellschaft DPG
IOP Institute of Physics

Published in partnership with: Deutsche Physikalische Gesellschaft and the Institute of Physics

OPEN ACCESS

RECEIVED
23 December 2021

REVISED
23 February 2022

ACCEPTED FOR PUBLICATION
9 March 2022

PUBLISHED
31 March 2022

Original content from this work may be used under the terms of the Creative Commons Attribution 4.0 licence.

Any further distribution of this work must maintain attribution to the author(s) and the title of the work, journal citation and DOI.

PAPER

Synchronization of a genetic oscillator with the cell division cycle

Gabriel Knotz[1,*], Ulrich Parlitz[1,2] and Stefan Klumpp[1,*]

[1] Institute for the Dynamics of Complex Systems, University of Göttingen, Friedrich-Hund-Platz 1, 37077 Göttingen, Germany
[2] Max Planck Institute for Dynamics and Self-Organization, Am Faßberg 17, 37077 Göttingen, Germany
[*] Authors to whom any correspondence should be addressed.

E-mail: g.knotz@theorie.physik.uni-goettingen.de and stefan.klumpp@phys.uni-goettingen.de

Keywords: genetic circuits, repressilator, synchronization, cell cycle

Abstract

Genetic circuits that control specific cellular functions are never fully insulated against influences of other parts of the cell. For example, they are subject to periodic modulation by the cell cycle through volume growth and gene doubling. To investigate possible effects of the cell cycle on oscillatory gene circuits dynamics, we modelled a simple synthetic genetic oscillator, the repressilator, and studied hallmarks of the resulting nonlinear dynamics. We found that the repressilator coupled to the cell cycle shows typical quasiperiodic motion with discrete Fourier spectra and windows in parameter space with synchronization of the two oscillators, with a devil's stair case indicating the Arnold tongues of synchronization. In the case of identical parameters for the three genes of the repressilator and simultaneous gene duplication, we identify two classes of synchronization windows, symmetric and asymmetric, depending on whether the trajectories satisfy a discrete three-fold rotation symmetry, corresponding to cyclic permutation of the three genes. Unexpectedly changing the gene doubling time revealed that the width of the Arnold tongues is connected to that three-fold symmetry of the synchronization trajectories: non-simultaneous gene duplication increases the width of asymmetric synchronization regions, for some of them by an order of magnitude. By contrast, there is only a small or even a negative effect on the window size for symmetric synchronization. This observation points to a control mechanism of synchronization via the location of the genes on the chromosome.

1. Introduction

Genetic circuits control many aspects of the behavior of a cell such as the adaptation of metabolism to available nutrients and the response to external stresses as well as developmental programs [1, 2]. In many cases, these circuits, which are based on products of genes controlling the activities of other genes, can be understood as deterministic or stochastic dynamical systems [3]. Particularly simple dynamical systems displaying, for example, bistability [4] or oscillations [5–7] have been designed in synthetic circuits, but often similar circuit designs also form the core of more complex native circuits.

However, one complication in understanding genetic circuits as simple dynamical systems is that they are never truly isolated systems, but rather coupled to processes going on in the background of the cell. Thus, a cell is not an inert 'chassis' for a genetic circuit, but its physiological state may affect the dynamics of that circuit in unexpected ways. One case where this coupling has been studied in some detail is the growth rate dependence of gene expression in bacteria [8], as in many cases the physiological state of a bacterium can be characterized by the growth rate [9–12]. Most interestingly, growth effects can mediate feedbacks, which may result in bistability that is absent without such coupling [8, 13, 14].

Another background process to which genetic regulatory dynamics is unavoidably coupled is the cell division cycle [15–17]. Again, this is particularly simple in bacteria, where the cell cycle affects the concentration of any protein via dilution by volume growth and via the doubling of the gene encoding that protein. These two effects result in a periodic modulation of the protein's concentration, which may be

© 2022 The Author(s). Published by IOP Publishing Ltd on behalf of the Institute of Physics and Deutsche Physikalische Gesellschaft

amplified by gene regulation [18]. A periodic modulation of the concentration by the cell cycle has been observed in yeast [19] and *Escherichia coli* [20]. If genes are replicated at different times in the division cycle, the resulting imbalance in stoichiometry of the corresponding proteins can trigger signaling [17] as proposed for the induction of sporulation in *Bacillus subtilis* [21].

Since the division cycle is a periodic perturbation of the dynamics of genetic circuits, its influence on circuits with oscillatory dynamics is of particular interest, as interaction of two oscillators may result in synchronization [22, 23]. If an oscillating circuit synchronizes to the cell cycle, this could be considered a strong perturbation, specifically if the oscillator's period is relevant for its function, raising the question whether oscillations are robust against the perturbation by the division cycle. On the other hand, in some situations synchronization may be functionally desirable, there are for example reports that the mammalian circadian clock and the cell division cycle are synchronized [24]. The simplest genetic oscillator is the repressilator, a synthetic bacterial genetic circuit of three transcription factors with cyclic repression [5, 7]. In an early model for cell cycle effects it was found that the repressilator is only mildly affected by the division cycle with a modulation of the amplitude [18]. Paijmans *et al* [25] later showed that synchronization of the repressilator with the division cycle can be observed, however only in small parameter windows. These synchronization windows became bigger when the genes are duplicated at different times [25]. Moreover, another design of a genetic oscillator [6] showed more pronounced synchronization with the division cycle [25]. An experimental test of synchronization between a genetic oscillator and the bacterial cell division cycle did not show synchronization, unless a backcoupling was introduced via a control of cell cycle protein by the oscillator to obtain mutual entrainment [26].

Here we revisit synchronization of the repressilator with the cell division cycle by analyzing the synchronization windows in more detail. We find that in the symmetric case where the three proteins are characterized by the same parameters and the same gene duplication times, there are two types of synchronization windows that reflect the cyclic symmetry of the system in different ways. Moreover, when the symmetry between the three proteins is broken by duplicating the genes at different times in the cell division cycle, the two types of synchronization windows show different behavior: large increases of the width of the synchronization windows are only seen in the case of asymmetric synchronization. This observation suggests a relation between a discrete symmetry of the trajectories and the efficiency of synchronization as reflected in the width of the synchronization regions. From the point of view of optimizing synchronization, maximizing the width of the synchronization window is one of several possible target features [27] (others include the speed of entrainment [28] or phase resetting [29, 30]). Our results point towards an intriguing connection with the symmetry properties of the trajectories and suggest that the timing of gene duplication can play a role in such optimization for genetic oscillators.

2. Cell cycle dependent repressilator

2.1. Repressilator without explicit coupling to cell cycle

The repressilator is a synthetic gene network of three transcription factors with circular repression as shown in figure 1(a). We start from a description of the production and degradation of a single protein expressed from an unregulated gene. The copy number of that protein per cell is denoted by P. Its dynamics is given by

$$\dot{P} = \alpha \cdot g - \beta \cdot P \tag{1}$$

with the synthesis and degradation rates α and β, respectively, and the gene copy number g. This equation can be derived from a system of equations describing the copy numbers of the protein and the corresponding mRNA (also used in earlier studies of the repressilator [5, 25]) by taking the mRNA dynamics to be in its steady state, as mRNA dynamics is typically faster than protein dynamics due to the short lifetime of mRNA [2, 15]. At cell division, which we will consider below, the protein copy number is halved.

Next we need to model the repression of protein production. A common approach is to describe repression by a Hill function

$$R([P]) = \frac{1}{1 + \left(\frac{[P]}{K}\right)^n}, \tag{2}$$

which multiplicatively modulates the synthesis rate. $R([P])$ describes the activity of the repressed gene as a function of the repressor concentration $[P]$ in relation to a reference concentration K and the Hill coefficient n. Because the Hill function depends on the concentration of the repressor, $[P] = P/V$ with cell

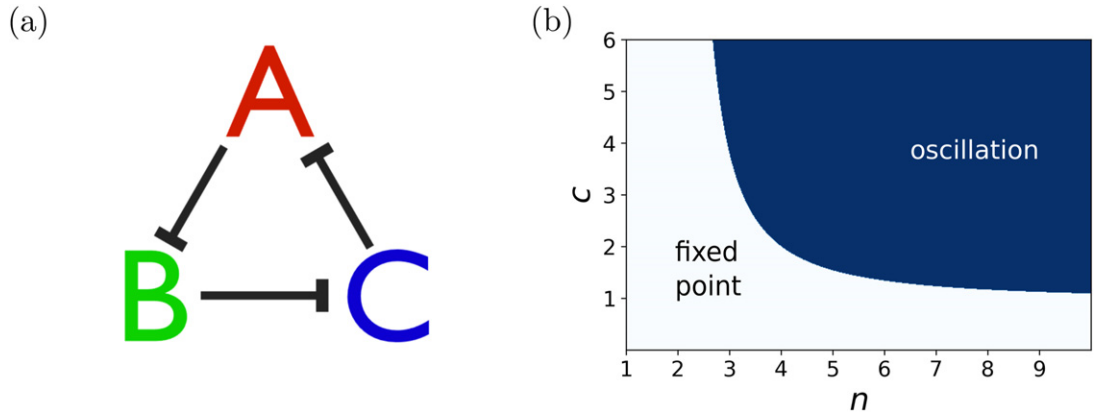

Figure 1. (a) Schematic diagram of the repressilator. The three proteins A, B and C repress each other in a cyclic manner. (b) Stability diagram of the free repressilator. In the stable regime the fixed point of the repressilator is stable. By increasing the Hill coefficient n or the dimensionless quantity $c = \frac{\alpha[g]}{\beta_{\text{eff}}K}$ the fixed point becomes unstable and trajectories converge towards a stable limit cycle.

volume V, we rewrite equation (1) as

$$[\dot{P}] = \frac{\mathrm{d}}{\mathrm{d}t}\left(\frac{P}{V}\right) = \frac{\dot{P}}{V} - \frac{\dot{V}}{V}\frac{P}{V}. \tag{3}$$

This expression shows that equations for concentrations have the same form as the corresponding equation for protein copy number with two modifications: the gene copy number g is replaced by the gene concentration $[g] = g/V$ (alternatively, a factor V^{-1} is often absorbed into α, which then becomes a synthesis rate per volume) and the degradation rate β is increased by the dilution term $\dot{V}/V$. Importantly, concentrations are not affected by cell division, as in cell division both volume and protein copy numbers are halved, so the concentration is continuous at the times of cell division [15].

If the cell cycle is not considered explicitly, one can approximate the volume as time independent and take cell cycle effects into account in an implicit fashion through the two modifications of the equation discussed above. This has been done in many studies of gene regulatory systems and will be used as a reference system here (free repressilator with implicit cell division). In that case, the dynamics of the repressilator with its cyclic repression of three genes can be expressed by the following system of coupled differential equations

$$\begin{aligned}
[\dot{P}_1] &= \alpha_1 \cdot R([P_3]) \cdot [g] - \beta_{\text{eff},1}[P_1] \\
[\dot{P}_2] &= \alpha_2 \cdot R([P_1]) \cdot [g] - \beta_{\text{eff},2}[P_2] \\
[\dot{P}_3] &= \alpha_3 \cdot R([P_2]) \cdot [g] - \beta_{\text{eff},3}[P_3]
\end{aligned} \tag{4}$$

with the constant average gene concentration $[g]$ and effective degradation rates $\beta_{\text{eff},i} = \beta_i + \dot{V}/V$ (for $i = 1, 2, 3$) that include the dilution term with the average volume growth rate $\dot{V}/V$ (which below we will specify for exponential growth as $\dot{V}/V = \ln 2/T$).

For simplicity we will consider the symmetric system with $\alpha_1 = \alpha_2 = \alpha_3 = \alpha$ and $\beta_1 = \beta_2 = \beta_3 = \beta$ (and, thus, $\beta_{\text{eff},i} = \beta_{\text{eff}} = \beta + \dot{V}/V$) and only introduce an asymmetry in the gene replication times towards the end of the paper.

The repressilator as defined by equation (4) is a dissipative system with a single fixed point. In the symmetric case that fixed point is given by $[P_1] = [P_2] = [P_3] = pK$ where $p > 0$ is determined by the implicit equation $p = c/(1 + p^n)$ with the dimensionless constant $c = \frac{\alpha[g]}{\beta_{\text{eff}}K}$, which describes the ratio of the concentration obtained by unregulated gene expression ($\alpha[g]/\beta_{\text{eff}}$) and the threshold concentration for repression, K.

Standard linear stability analysis shows [31] that the fixed point is stable for small c and becomes unstable through a Hopf bifurcation at a critical value of c, which depends on the Hill coefficient n and for large n is $\approx$1. In the unstable regime, the repressilator develops stable relaxation oscillations.

A map of a stable and unstable regime of the oscillator is shown in figure 1(b).

Typical trajectories of the three proteins in the oscillating regime are shown in figure 2 and will be compared to the case, where the repressilator is explicitly coupled to the cell cycle below.

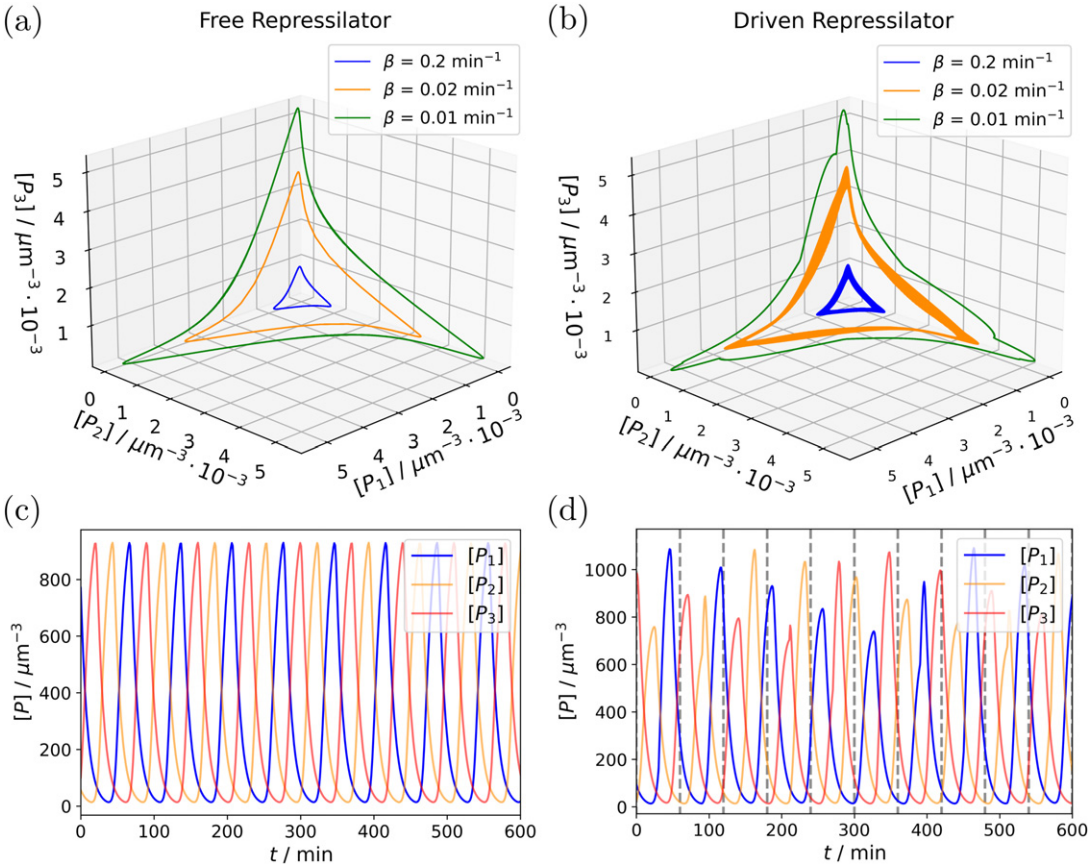

Figure 2. Trajectories of the repressilator (a) and (c) without and (b) and (d) with explicit coupling to the cell cycle with $T = 60$ min. The grey vertical lines in (d) indicate the times of cell division and, thus, the periodic driving of the repressilator. In (a) and (c), cell cycle effects are included implicitly through a constant average gene concentration $[g] = \frac{1}{V_0}\frac{1}{\sqrt{2}\ln 2}$ and an effective degradation rate $\beta_{\text{eff}} = \beta + \frac{\ln 2}{T}$ that includes dilution due to volume growth. In (a) and (b) for different β and in (c) and (d) with $\beta = 0.2$ min^{-1}. The free repressilator in the oscillatory regime develops stable oscillations whereas the trajectories of the driven repressilator typically covers a broader region in the phase space, for example for $\beta = 0.2$ and 0.02 min^{-1} (blue and orange in (b). However, one can get stable periodic trajectories as well, e.g. for $\beta = 0.01$ min^{-1} (green).

2.2. Cell cycle effects

The cell cycle provides a periodic modulation of parameters of the repressilator and thus an external driving force for the oscillator. To implement the cell cycle into our model explicitly, we introduce two effects. The first one is the volume growth and division of the cell. The cell volume grows exponentially [32] and after a period of the cell cycle of time T, the cell is twice as big as at the beginning of the cell cycle. At that time, the cell divides and the volume is set back to its initial value. As a side remark, we note that the difference between linear and exponential volume growth is rather small for such a model for protein synthesis [15]. To simplify the expressions for cell cycle-dependent parameters, we introduce a second time variable $\tau = t \bmod T$, the age of the cell, which measures the time since the last division. Divisions are taken to occur at times nT with integer n, corresponding to $\tau = 0$.

The second effect is the gene doubling. At times $\tau = t_{\text{d}}$, all three genes of the repressilator are duplicated simultaneously. This is a good assumption if the genes are close together on the chromosome, but there may be significant impact if that is not the case, as shown in reference [25] and discussed further in section 3.3. At cell division, $\tau = 0$, the copy number of all genes is reduced again to a single copy. Like for proteins, the concentrations of the genes are continuous at times of division.

All in all we get the following equations for the cell cycle effects

$$V(t) = V_0 \exp\left(\frac{\tau \ln 2}{T}\right) \tag{5}$$

$$g(t) = \begin{cases} 1 & 0 \leqslant \tau < t_{\text{d}} \\ 2 & t_{\text{d}} \leqslant \tau < T, \end{cases} \tag{6}$$

where both the cell's volume V and the gene copy number g depend on time via the cell's age $\tau = t \bmod T$. As a consequence, the equation for the dynamics of the concentration of an unregulated protein takes the form

$$[\dot{P}] = \alpha \left[g\right](t) - \left(\beta + \frac{\ln 2}{T}\right)[P]\,. \tag{7}$$

Importantly, the gene concentration

$$\left[g\right](t) = \frac{g(t)}{V(t)} = \begin{cases} \frac{1}{V_0} \exp\left(-\frac{\tau \ln 2}{T}\right) & 0 \leqslant \tau < t_\mathrm{d} \\ \frac{2}{V_0} \exp\left(-\frac{\tau \ln 2}{T}\right) & t_\mathrm{d} \leqslant \tau < T, \end{cases} \tag{8}$$

is time dependent and acts as a driving oscillator with unidirectional coupling. At the gene doubling time t_d the production rate $\alpha\left[g\right]$ will increase by a factor of two, initiating a phase of increased protein production. In addition, the dilution term added to the degradation rate β takes the form $\frac{\ln 2}{T}$ due to the exponential volume growth with doubling time T.

Likewise, the repressilator driven by the cell cycle takes the form

$$\begin{aligned} [\dot{P}_1] &= \alpha_1 \cdot \frac{1}{1 + \left(\frac{[P_3]}{K}\right)^n} \cdot \left[g\right](t) - \left(\beta_1 + \frac{\ln 2}{T}\right)[P_1] \\ [\dot{P}_2] &= \alpha_2 \cdot \frac{1}{1 + \left(\frac{[P_1]}{K}\right)^n} \cdot \left[g\right](t) - \left(\beta_2 + \frac{\ln 2}{T}\right)[P_2] \\ [\dot{P}_3] &= \alpha_3 \cdot \frac{1}{1 + \left(\frac{[P_2]}{K}\right)^n} \cdot \left[g\right](t) - \left(\beta_3 + \frac{\ln 2}{T}\right)[P_3]\,, \end{aligned} \tag{9}$$

where we have inserted the repression function from equation (2) and where $\left[g\right](t)$ is given by equation (8). Below, we will again use symmetric rate constants $\alpha = \alpha_1 = \alpha_2 = \alpha_3$ and $\beta = \beta_1 = \beta_2 = \beta_3$.

The equations of motion as described so far are integrated numerically with the standard SciPy RK23 integrator. For numerical examples we choose $\alpha = 60\ \mathrm{min}^{-1}$, $K = 50\ \mu\mathrm{m}^{-3}$, $V_0 = 0.5\ \mu\mathrm{m}^{-3}$ and $n = 4$ unless stated otherwise. The gene doubling time t_d is set to $\frac{T}{2}$.

Example trajectories with and without the coupling to the cell cycle are shown in figure 2. The repressilator with implicit cell cycle exhibits stable oscillations (all trajectories shown here are for parameters in the oscillating regime), corresponding to a simple limit cycle. By contrast, the trajectories of the repressilator driven by the cell cycle are more complex. The oscillations show additional frequencies, reflected in a modulation of the amplitudes of the three concentrations. In the three-dimensional phase space the region occupied by the trajectories generally become broader, like for example for $\beta = 0.2$ and $0.02\ \mathrm{min}^{-1}$ (blue and orange trajectories in figure 2(b); the Fourier spectra discussed below indicate that these trajectories are quasiperiodic, thus the blue and orange trajectories cover the projection of a torus-like object). However, for some parameter values, one can also get simple limit cycles as shown for $\beta = 0.01\ \mathrm{min}^{-1}$ (green trajectory in figure 2(b)).

3. Synchronization with the cell cycle

3.1. Period and power spectrum of the driven oscillator

To obtain the frequency of the repressilator coupled to the cell division cycle, we introduce a phase variable and measure its derivative. To that end, we compute the analytic signal, a complex valued representation of the original signal, $H(s(t)) = s(t) + ih(s(t))$, with the real part given by the original signal $s(t)$, here with $s(t) = [P_1]$, and the imaginary part by its Hilbert transform

$$h(s(t)) = \frac{1}{\pi} \int_{-\infty}^{\infty} \frac{s\left(t'\right)}{t - t'}\,\mathrm{d}t'. \tag{10}$$

An instantaneous phase $\phi(t)$ can then be obtained by representing the analytic signal by

$$H(s(t)) - z_0 = A(t)\mathrm{e}^{\mathrm{i}\phi(t)} \tag{11}$$

with a properly chosen origin z_0. For a periodic or quasi-periodic oscillator, the analytic signal represented in the complex plane typically resembles a circle as shown for the repressilator in figure 3(a), so a linear fit to the phase $\phi(t)$ provides a well-defined average frequency.

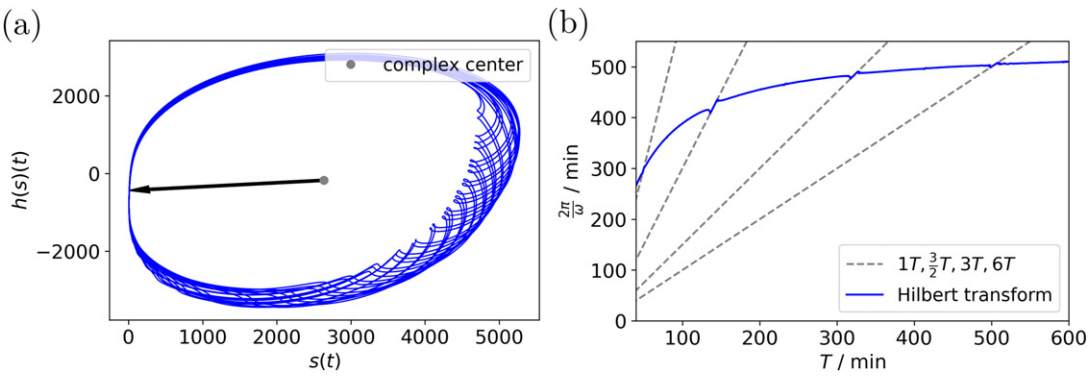

Figure 3. (a) Analytic signal for the repressilator with $\beta = 0.011\ \text{min}^{-1}$, $T = 60$ min. (b) Average period of the repressilator determined via the Hilbert transform with $\beta = 0.0215\ \text{min}^{-1}$ for multiple cell division times T. One notices that there are regions where the period follows straight lines starting from the origin.

Figure 3(b) shows the period measured in this way as a function of the cell cycle time T. Superimposed on an overall increase, we obtain characteristic windows, in which the dependence on T is linear, indicating synchronization of the repressilator with the cell cycle, for example around $T = 400$ min and $T = 150$ min, in agreement with earlier results [25]. The most prominent ones among those linear segments have simple integer or rational slopes as indicated by the dashed lines in figure 3(b).

We note that the Hilbert transform is not the only option for determining the phase. For example, a phase can also be extracted by projecting the dynamics in the three-dimensional space of the three concentrations onto a suitable two-dimensional subspace in which again a circle-like orbit is obtained (we used the projection $y_1 = -2[P_1] + [P_2] + [P_3]$, $y_2 = [P_2] - [P_3]$ and obtained the same results). The advantage of the Hilbert transform is that it only needs the time series of one of the variables, so it can also be applied to experimental data if only one of the concentrations is observed with a fluorescence reporter. We further note that the period determined via the Hilbert transform agrees with the dominant period obtained from the power spectrum (see below), while the average peak-to-peak time, which was used in reference [25], systematically underestimates the period, as shown in the appendix A. Finally, to determine only the period without the phase, one can also use the zero crossings of a shifted time series and get the same results as with the Hilbert transform (see appendix A).

Figure 4(a) shows a full power spectrum of the oscillation. For comparison, the power spectrum of the free repressilator is also included. Some prominent peaks of the driven spectrum are seen to coincide between the two spectra. The position of the dominant peaks can be approximated by

$$\omega \approx |n \cdot \omega_{\text{cell}} + m \cdot \omega_{\text{free}}| \tag{12}$$

with integers n, m as indicated in figure 4(a) by the dashed vertical lines. While this expression is not exact, it provides a rather accurate approximation of the position of the peaks. The two frequencies in this approximation, ω_{cell} and ω_{free}, correspond to the two uncoupled oscillators, i.e. the cell cycle and the free repressilator (with implicit cell division). More precisely, ω_{free} is the frequency of an free repressilator with the average gene concentration $\langle [g] \rangle = \frac{1}{T}\int_0^T [g] = \frac{1}{V_0}\frac{1}{\sqrt{2}\log 2}$. Such a behaviour is typical for quasi-periodic motion [22]. The power spectrum also provides a quantitative description of the modulated oscillations observed in earlier studies [18]. The highest peak of the spectrum is seen to be the one with the lowest frequency among those peaks without a contribution from the cell cycle frequency, i.e. the peak with $n = 0, m = 1$ in equation (12). Its frequency (which is approximately, but not exactly that of the free repressilator) agrees with the frequency obtained from the Hilbert transform.

Figure 4(a) compares the power spectra of the driven and free repressilator. The dominant peaks of the two spectra coincide. This observation suggests already that the influence of the cell cycle on the frequency of the repressilator is small enough that it can often be neglected. Indeed, if we directly measure the period of the driven and free repressilator and compare them (figure 4(b)), the difference is seen to be small, apart from certain areas in parameter space, where the driven repressilator speeds up and slows down quite rapidly.

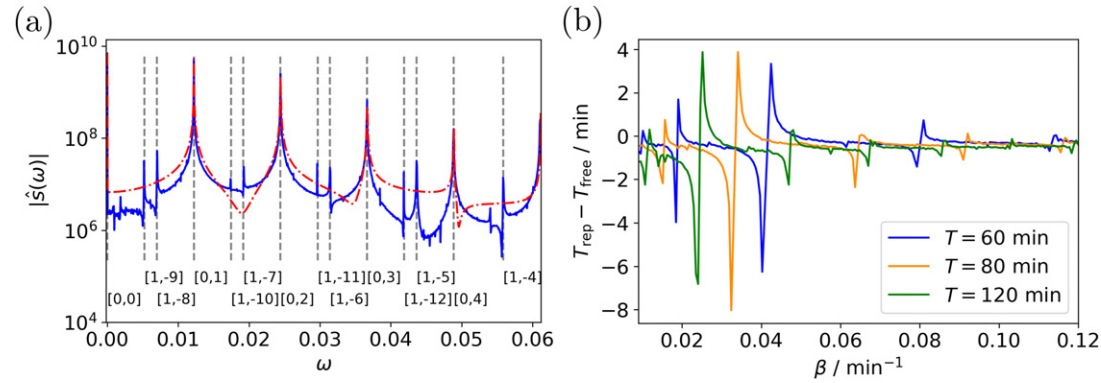

Figure 4. (a) A power spectrum of a repressilator with $\beta = 0.011$ min^{-1}, $T = 60$ min. Additionally the dashed vertical lines correspond to frequencies $|n\frac{2\pi}{T} + m\frac{2\pi}{T_{\text{free}}}|$ with T_{free} the period of a corresponding free repressilator. In the graph they are labeled as $[n, m]$. The red dashed line is the power spectrum of the corresponding free repressilator. (b) The difference between the period determined for the driven and the free repressilator. Overall the difference between both oscillators is rather small, apart from areas where the driven repressilator speeds up and slows down again rapidly. After that the difference converges for increasing β to a smaller value.

3.2. Two types of synchronization

To further analyze the dynamics in the windows in which the observed period shows a linear dependence on the division time T, we plot the period (figure 5(a)) together with an orbit diagram in figure 5(b). In this diagram, we display the values taken by the concentration $[P_1(nT)]$ at integer multiples of the cell division time as a function of the division time T. Synchronization with the cell division cycle at a given T (and thus periodic dynamics of the full system) is seen as a discrete set of values that repeat after a finite number of cycles, while without synchronization (quasiperiodic dynamics of the full system) a continuous distribution of values is obtained. The comparison reveals that the trajectories of the oscillator become periodic in the windows with the linear dependence of the period on the division time. For the parameters used here (with a realistically small degradation rate $\beta = 0.01$ min^{-1}), the biggest interval with periodic behavior is seen around $T = 352$–375 min, which corresponds to very slow cell growth, but two smaller windows around $T = 60$ min and $T = 130$ min are in the range accessible for the growth of *E. coli* with common growth media. As observed above, in the windows with linear dependence, the period of the repressilator is locked to rational multiples of the cell division time T. For the three mentioned windows, the dependencies are $3T$, $6T$ and $9T$, respectively. Another small window near $T = 215$ min shows a $\frac{3}{2}T$ dependence (inset in figure 5(a)). The observed locking of the repressilator period to the cell cycle together with the periodic orbits seen in the Poincare maps indicate the synchronization of the repressilator with the cell cycle.

Another hallmark of synchronization can be obtained from the phase $\phi(t)$ extracted from the Hilbert transform. By calculating the winding number

$$\Omega = \lim_{n\to\infty} \frac{\phi(n \cdot T) - \phi(0)}{n} \tag{13}$$

one obtains areas of synchronizations in parameter space, also called Arnold tongues, as areas of constant winding number. In the plot of the winding number (figure 5(c)), these areas appear as intervals of constant winding number that correspond to the windows of linear dependence in figure 5(a) and the windows of periodic dynamics in the orbit diagram (figure 5(b)). The values of the winding number in these intervals are given by the inverse of the slope of the linear dependence of the period on the division time. The winding number, which indicates the ratio of the driven repressilator frequency to the driving frequency of the cell cycle, allows for a geometric interpretation of synchronization [22, 33]: it indicates the number of full turns of one oscillator in one period of the other oscillator. An integer or rational value as in the synchronization windows thus distinguishes periodic from quasiperiodic motion of the coupled system. As the orbit of two oscillators is located on a torus, the former case is characterized by a closed orbit on that torus, while in the latter case, the orbit 'fills' the whole torus [22, 33].

Figure 6 shows trajectories in the synchronization windows and also indicates the times of gene doubling and cell division. Based on these trajectories, we distinguish two types of synchronization, to which we refer as symmetric and asymmetric. For the symmetric case, the stable trajectory is invariant under cyclic permutation of the proteins, so

$$\text{(A,B,C)} \to \text{(B,C,A)} \to \text{(C,A,B)} \to \text{(A,B,C)}\,. \tag{14}$$

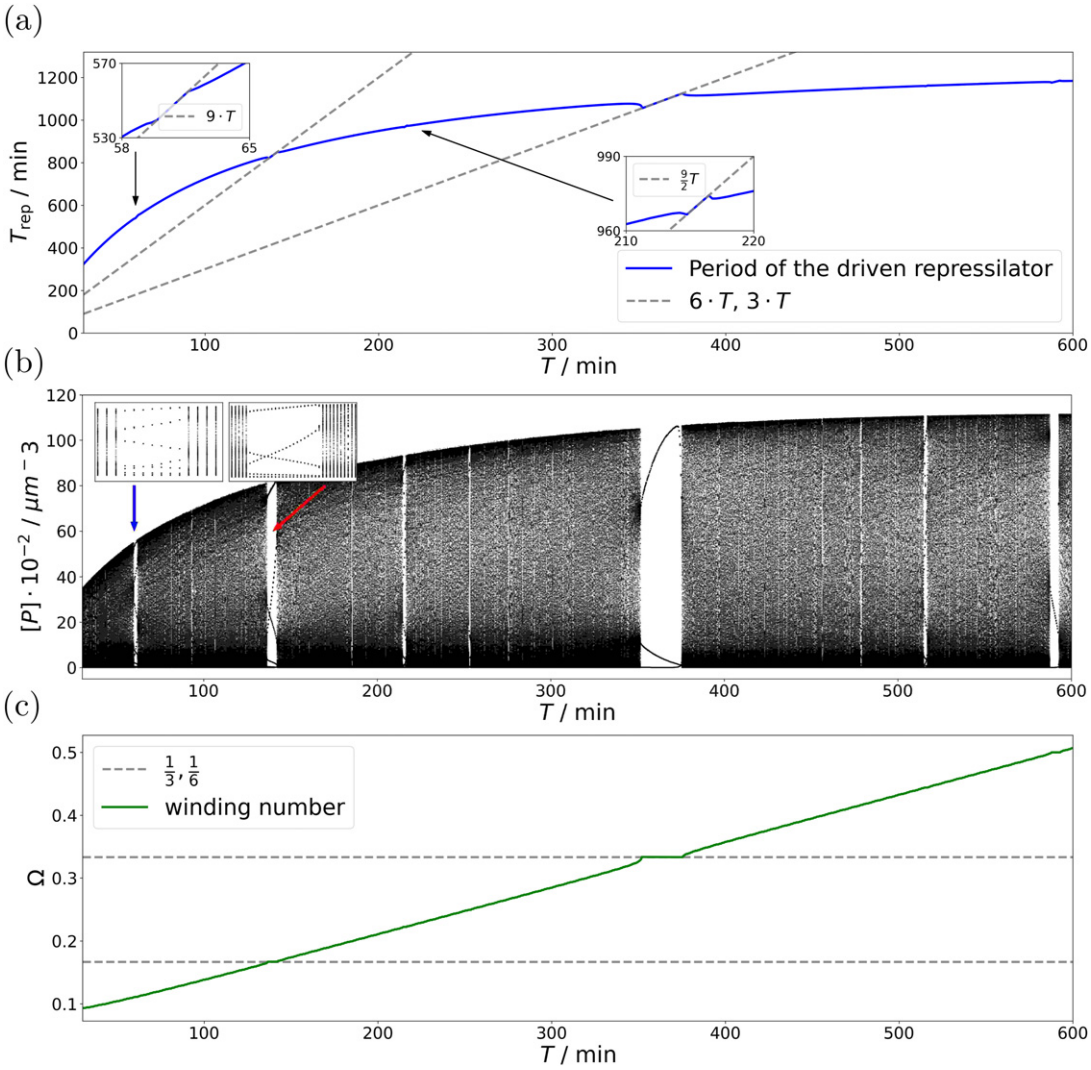

Figure 5. Multiple graphs for a repressilator with $\beta = 0.01\ \text{min}^{-1}$ for changing cell division times T. In (a) the period determined via the Hilbert transform, in (b) an orbit diagram with the current protein concentration at times $n \cdot T$ with $n \in \mathbb{N}$ and in (c) the winding number calculated from the phase of the Hilbert transform. The insets in (b) show a period 9 (blue) and period 6 (red) window. Note that some values are barely distinguishable in this visualization. The most important feature is that areas of synchronizations in (a) correspond to periodic windows in (b) and to plateaus in (c). The value of the winding number in Arnold tongues is the same as the inverse slope of the synchronization straights in (a).

This is equivalent to a three-fold discrete rotation symmetry of the trajectory around the $(1, 1, 1)$ axis. Reflecting this symmetry, in the corresponding synchronization windows the linear relation between the period of the repressilator and the cell division time takes the form $T_{\text{rep}} = \frac{3n}{m}T$ with coprime positive integers n, m.

The largest sychronization windows discussed above (and indicated in figure 5) are of this type. All synchronization windows that do not show this permutation or discrete rotation symmetry are referred to as asymmetric. An example is the window with $T_{\text{rep}} = 1T$ (figure 6(a)).

3.3. Synchronization for non-simultaneous duplication of the three genes

Pajimans *et al* observed that synchronization of the repressilator with the cell cycle becomes more pronounced when the genes are not duplicated at the same time [25]. Duplication at different times in the division cycle is obtained if the three genes are in different locations on the chromosome. Indeed, if we shift the gene doubling time of protein A relative to the other two proteins B and C, some of the most pronounced synchronization windows get bigger and many small windows become more apparent in the orbit diagram based on the Poincaré map (figure 7(a), varying T) as well as in the plot of the frequency as a function of the degradation rate β (figure 7(b)). This is shown in figure 7(b), where we compare the case where all three genes are duplicated at $\tau = t_{\text{d}} = T/2$ with the case where gene A is duplicated 20 min earlier. Here and in the following figures we plot the frequency of the repressilator as a function of the degradation rate β (which modulates the frequency of the free repressilator) rather than as a function of

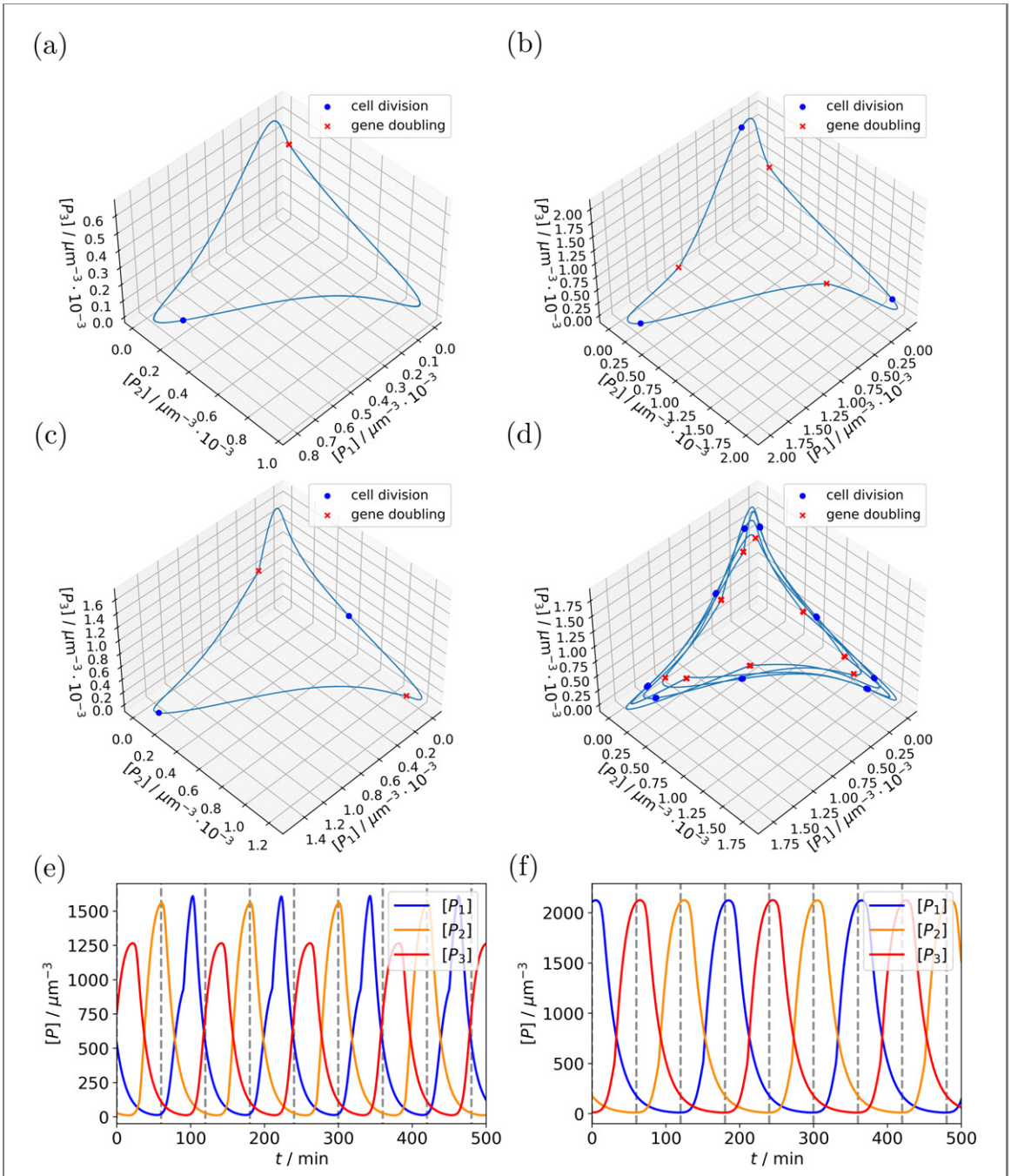

Figure 6. Example trajectories for asymmetric (a), (c) and (e) and symmetric synchronization orbits (b), (d) and (f). The synchronization $1T$ (a) and $2T$ (c) are not symmetric under cyclic permutation of the protein coordinates, which can easily be seen by the position of the gene doubling (red cross) or the cell division (blue dot) in the synchronization trajectory. For the $3T$ (b) and $\frac{9}{4}T$ (d) orbit this condition is fulfilled, even though this might be not so obvious for the latter. (e) and (f) Show time representations for the asymmetric orbit $2T$ and the symmetric orbit $3T$, respectively. Here, the vertical dashed lines indicate the times of cell division.

the cell division time to avoid complications when the earlier duplication time approaches the beginning of the cell cycle. The most prominent examples for synchronization becoming more pronounced are the $1T$ and $2T$ windows. However, not all synchronization windows get bigger, the $3T$ window, for example, actually gets smaller.

The different responses of the synchronization windows to the shift of the gene doubling time of one protein are illustrated in figure 7, where we plot two of the synchronization windows as function of the shift in the duplication time for shifts ranging between the two extremes shown in figures 7(c) and (d). The $3T$ window is seen to decrease in size, while the $2T$ window increases. The two cases correspond to a symmetric and an asymmetric synchronization scenario, respectively, as shown by the trajectories in figure 6.

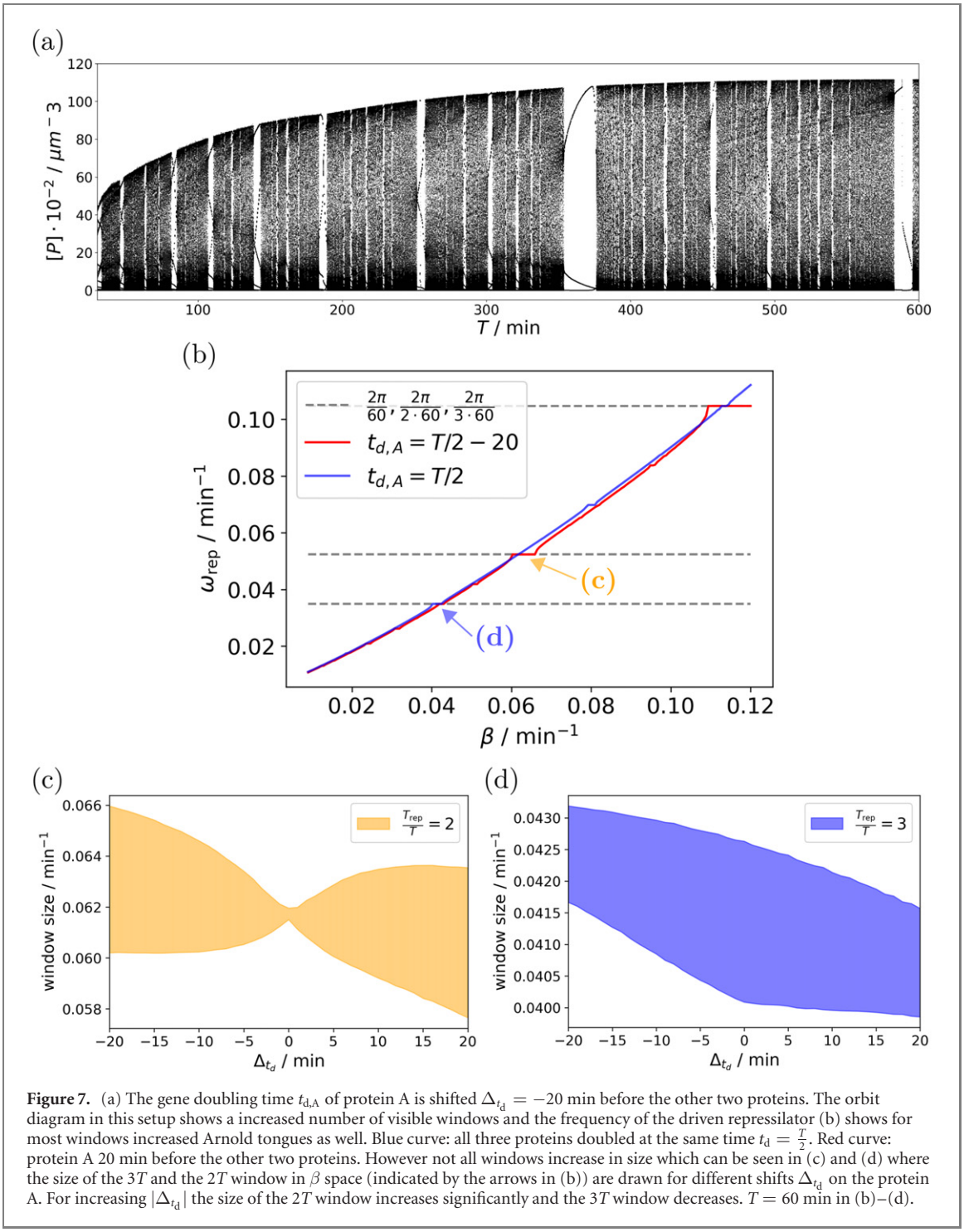

Figure 7. (a) The gene doubling time $t_{\mathrm{d,A}}$ of protein A is shifted $\Delta_{t_\mathrm{d}} = -20$ min before the other two proteins. The orbit diagram in this setup shows a increased number of visible windows and the frequency of the driven repressilator (b) shows for most windows increased Arnold tongues as well. Blue curve: all three proteins doubled at the same time $t_\mathrm{d} = \frac{T}{2}$. Red curve: protein A 20 min before the other two proteins. However not all windows increase in size which can be seen in (c) and (d) where the size of the $3T$ and the $2T$ window in β space (indicated by the arrows in (b)) are drawn for different shifts Δ_{t_d} on the protein A. For increasing $|\Delta_{t_\mathrm{d}}|$ the size of the $2T$ window increases significantly and the $3T$ window decreases. $T = 60$ min in (b)–(d).

To test whether there is a general relation between the type of the synchronization and the response to the shift in the duplication time (which breaks the symmetry between the three proteins), we consider the sizes of the 28 synchronization windows that can be identified in figure 7. We determine the window size (in the space of degradation rates β and for $T = 60$ min) for synchronous gene doubling at $t_\mathrm{d} = \frac{T}{2}$ and for a shift of 20 min applied to the gene doubling time of the A protein. The results are shown in figure 8, where we plot the window size with the shift against that without the shift. Windows of asymmetric synchronization are shown as circles, those corresponding to symmetric synchronization as crosses. The dashed line indicates unchanged window size. Strikingly, all windows corresponding to asymmetric synchronization are above the dashed line and thus get bigger upon the shift, some of them increase by more than a factor 10. By contrast, the windows corresponding to symmetric synchronization lie very near the dashed line or even below it. These results thus suggest that asynchronous gene doubling can indeed make synchronization more pronounced, but only for cases of asymmetric synchronization, while the effect

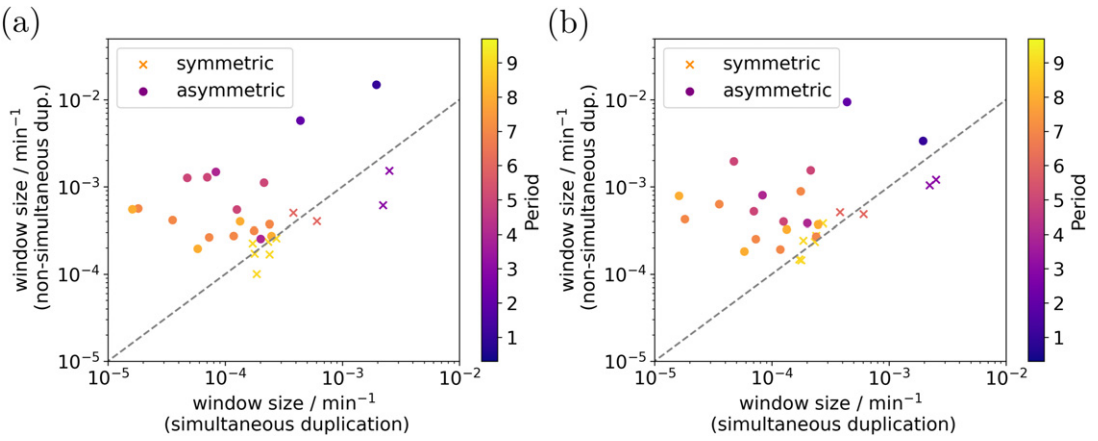

Figure 8. Each marker represents a synchronization window which can be found in figure 7(b). On the x-axis we have the size of the synchronization window in β space with synchronous gene doubling at $\frac{T}{2}$ and on the y-axis the window size with a shift on the gene doubling time of protein A by $\Delta_{t_d} = -20$ min (a) or with gene doubling times $\tau_A = 10$ min, $\tau_B = 30$ min and $\tau_C = 50$ min (b). Every synchronization window above the grey dotted line does increase with the shift and every window below the line decreases. The crosses correspond to symmetric synchronizations and the dots to asymmetric synchronizations. The color of each dot indicates the period of the window, that can be found in an orbit diagram.

on symmetric synchronization is small or even negative. To test whether there is a dependence on the period of the synchronized orbits, we indicated the period by the color of the symbols, but no obvious pattern is seen.

As a further test of this hypothesis, we shifted the doubling not only of one gene, but of two away from $t_d = T/2$ and repeated the analysis. Figure 8(b) shows the size of the synchronization windows for the case where gene A is duplicated 20 min earlier and gene C 20 min later than gene B. The overall picture is the same: breaking the symmetry by shifted gene duplication times increases the size of synchronization windows for asymmetric synchronization, with big increases for some of them, but has only a small positive or negative effect for symmetric synchronization.

4. Discussion

Genetic circuits are generically coupled to a periodic forcing by the cell division cycle via volume growth and gene duplication. Here we have studied the specific case of how this coupling affects a genetic oscillator, the repressilator. In agreement with earlier studies [18, 25], we see that the perturbations of the repressilator oscillations are mostly moderate. However, there are distinct windows in the parameter space in which the two oscillators are synchronized. Some of these windows occur in accessible parameter ranges and should thus be experimentally observable. Importantly, however, the coupling to the cell division cycle as studied here applies to the case where the repressilator genes are located on the chromosome. If the repressilator is encoded on a plasmid, the coupling will be different and should typically be weaker due to asynchronous duplication of multiple copies of the plasmid. In the context of synthetic circuits, this suggests that depending on whether one is interested in the periodic forcing by the cell cycle as a feature or whether one considers it rather as a perturbation, implementation strategies using the chromosome may or may not be preferable over strategies based on plasmids.

We note that a number of studies have emphasized the competition between genes and allocation of gene expression machinery [11, 34, 35], including recent work on cell cycle effects [16]. In the description used here, we have not included such effects, as they can be neglected if the genes considered account only for a small fraction of the total transcriptome and proteome. Specifically, Lin and Amir [16] have proposed that instead of the gene copy number g_i of a gene i, the gene fraction, $g_i/\sum_j g_j = g_i/(g_i + \sum_{j\neq i} g_j)$, where the sum runs over all expressed genes, should be used in the transcription rate and likewise for mRNA fractions in the translation rate. If the gene of interest only contributes a small amount to these sums, however, the difference between the two descriptions is small. Specifically, transcription can be expected to be proportional to the gene copy number.

For the special case where the three proteins of the repressilator are characterized by the same parameters (synthesis and degradation rates, parameters of the Hill function), we have shown that the synchronization windows can be grouped into two classes: in one class, the periodic trajectories exhibit a three-fold discrete symmetry under cyclic permutation of the proteins and the number of cell division

cycles in one period is an integer multiple of 3. In the other class, there is no such symmetry and instead three periodic solutions exist that are shifted relative to each other. Unexpectedly, we found that the these two types of synchronization show different behavior when the symmetry between the parameters of the three proteins is broken by non-synchronous gene duplication: the synchronization windows without the permutation symmetry become wider, while those with that symmetry get smaller or remain unchanged. In general, the width of synchronization windows can be considered as a measure of the efficiency of entrainment and can be optimized by modulating the waveform of the periodic forcing [27], at least in the limit of weak forcing. Our observation indicates a relation between such optimal forcing and a discrete symmetry of the oscillation. Only synchronization windows corresponding to asymmetric synchronization show a potential for considerable improvement of the efficiency of entrainment. Whether such a relation holds more general than for the specific system studied here and how the symmetry of the trajectories influences the width of the synchronization regions remain to be investigated.

From the biological point of view, one can ask whether synchronization of a genetic oscillator with the cell cycle provides a benefit or rather a perturbation of the oscillators dynamics. Indeed, both scenarios are possible. Both eukaryotic and cyanobacterial circadian clocks have been shown to be coupled to the cell cycle, however the coupling is typically such that the two oscillators influence each other [24, 36]. Synchronization in that case can stabilize the oscillations and coordinate cellular functions with the day–night cycle. By contrast, if an oscillator has a precisely tuned function requiring a defined period, the coupling to the cell cycle amounts to an unwanted disturbance and insulating the oscillations against these perturbations may be crucial to their function. It has indeed be argued that some features of the cyanobacterial circadian clock serve exactly that function, for example multiple, independently replicated copies of the clock genes [37].

In summary, our results show that the generic coupling of genetic oscillators to the cell cycle due to discrete gene duplication events provides both a source of perturbations and an additional layer of control of the behavior of such genetic circuits. Synchronization with the division cycle occurs in typically small parameter regions, which may be optimized via the gene location on the chromosome, with an intriguing relation between synchronization efficiency and the symmetry of the oscillator's trajectories in phase space.

Acknowledgments

We acknowledge support by the Open Access Publication Funds of the University of Göttingen.

Data availability statement

The data that support the findings of this study are available upon reasonable request from the authors.

Appendix A. Determining frequencies

A previous study of synchronization of genetic oscillators with the cell cycle [25] used the mean peak-to-peak time, the time between local maxima of the trajectory, to determine the frequency of the oscillator. However, this approach is not generally applicable and may systematically underestimate the period of the driven repressilator: the increased protein production after gene doubling can lead to a rapid increase of protein concentration. If this increase happens near a maximum of the oscillations this can result in two closely spaced local maxima as shown in figure A1(a). This lowers the estimated period of the oscillations.

The period determined with the peak to peak method is plotted as a function of the cell cycle duration T in figure A1(b) (green line), together with the period obtain via the Hilbert transform (blue line). The peak to peak time can indeed be seen to be systematically smaller or at most equal to the period determined via the Hilbert transform. Moreover, the mean peak to peak time appears to be very unstable (green line) and fluctuates strongly. In addition, we plot the standard deviation of the peak-to-peak time (green area), which tends to be rather large and indicates the broad distribution of the individual peak-to-peak times. However, in the synchronization window, see here as intervals where the measured period increases in a linear fashion, the standard deviation is negligibly small and the peak-to-peak time is in agreement with the period calculated via the Hilbert transform.

In case of the sinusoidal-like oscillations of the protein concentrations (see figures 6(e) and (f)) an alternative method to determine an average period is to use the zeros crossings of a shifted time series. This method also avoids the problems of increased protein production after gene duplication. For this we shift

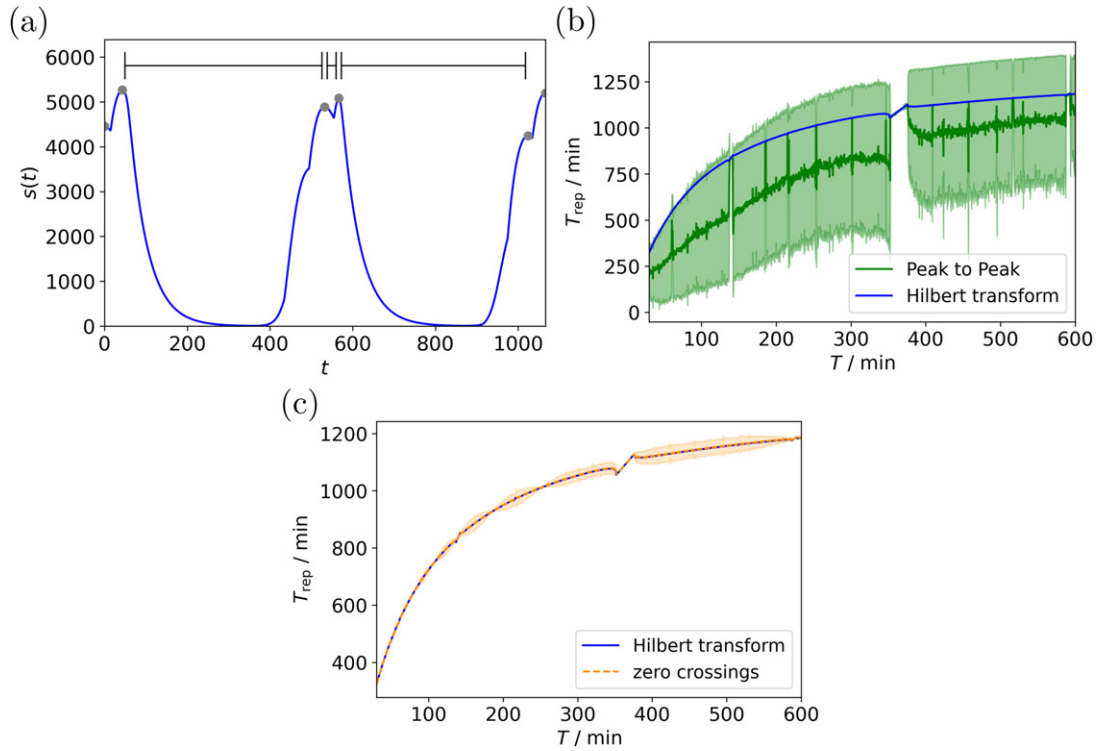

Figure A1. (a) Example trajectory of the repressilator with ($\beta = 0.011$ min^{-1}, $T = 60$ min). The local maxima can be very close together which leads to a systematic underestimation of the period. (b) Period of the repressilator determined by the peak to peak method for $\beta = 0.01$ min^{-1}. The green area displays the standard deviation for the mean of the local maxima and blue line is the period we obtained by the Hilbert transformation. When the repressilator synchronizes the peak to peak method and the Hilbert transformation give the same result. (c) Period determined by zero crossings of the time series from which the average of the maximal and the minimal value has been subtracted, again for $\beta = 0.01$ min^{-1}. The standard deviation (orange area) shows a similar behaviour as the peak to peak method, but is much smaller. The average itself gives the same results as the Hilbert transform.

the trajectory by the median value of the maximum and the minimum of the protein concentration and measure the distance between two zero crossings from negative to positive as period. Because this distance is not constant for quasiperiodic oscillations, we average over many crossings to get an average period. The results for different cell cycles T are shown in figure A1(c). With this method the average is much smoother (orange line) and agrees well with results obtained via the Hilbert transform (blue line). In addition, we can again observe how the standard deviation (orange area) is reduced in the regions corresponding to a periodic orbit.

ORCID iDs

Gabriel Knotz https://orcid.org/0000-0003-1485-9230
Ulrich Parlitz https://orcid.org/0000-0003-3058-1435
Stefan Klumpp https://orcid.org/0000-0003-0584-2146

References

[1] Ptashne M 1986 *A Genetic Switch: Phage Lambda and Higher Organisms* 2nd edn (Oxford: Blackwell)
[2] Alon U 2007 *An Introduction to Systems Biology: Design Principles of Biological Circuits* (Boca Raton, FL: CRC Press)
[3] Jeff H, David M, Farren I and Collins J J 2001 *Nat. Rev. Genet.* **2** 268–79
[4] Gardner T S, Cantor C R and Collins J J 2000 *Nature* **403** 339–42
[5] Elowitz M B and Leibler S 2000 *Nature* **403** 335–8
[6] Stricker J, Cookson S, Bennett M R, Mather W H, Tsimring L S and Hasty J 2008 *Nature* **456** 516–9
[7] Potvin-Trottier L, Lord N D, Vinnicombe G and Paulsson J 2016 *Nature* **538** 514–7
[8] Klumpp S, Zhang Z and Hwa T 2009 *Cell* **139** 1366–75
[9] Schaechter M, Maaløe O and Kjeldgaard N O 1958 *J. Gen. Microbiol.* **19** 592–606
[10] Bremer H and Dennis P 1996 Modulation of chemical composition and other parameters of the cell by growth rate *Escherichia Coli and Salmonella Typhimurium: Cellular and Molecular Biology* vol 2 ed F Neidhard (Washington DC: American Society for Microbiology) pp 1553–69
[11] Scott M, Gunderson C W, Mateescu E M, Zhang Z and Hwa T 2010 *Science* **330** 1099–102

[12] Jun S, Si F, Pugatch R and Scott M 2018 *Rep. Prog. Phys.* **81** 056601
[13] Tan C, Marguet P and You L 2009 *Nat. Chem. Biol.* **5** 842–8
[14] Klumpp S and Hwa T 2014 *Curr. Opin. Biotechnol.* **28** 96–102
[15] Marathe R, Bierbaum V, Gomez D and Klumpp S 2012 *J. Stat. Phys.* **148** 608–27
[16] Lin J and Amir A 2018 *Nat. Commun.* **9** 4496
[17] Slager J and Veening J.-W 2016 *Trends Microbiol.* **24** 788–800
[18] Bierbaum V and Klumpp S 2015 *Phys. Biol.* **12** 066003
[19] Cookson N A, Cookson S W, Tsimring L S and Hasty J 2010 *Nucleic Acids Res.* **38** 2676–81
[20] Walker N, Nghe P and Tans S J 2016 *BMC Biol.* **14** 11
[21] Narula J, Kuchina A, Lee D-y D, Fujita M, Süel G M and Igoshin O A 2015 *Cell* **162** 328–37
[22] Pikovsky A, Rosenblum M and Kurths J 2001 *Synchronization: A Universal Concept in Nonlinear Sciences* (Cambridge: Cambridge University Press)
[23] Strogatz S H and Stewart I 1993 *Sci. Am.* **269** 102–9
[24] Bieler J, Cannavo R, Gustafson K, Gobet C, Gatfield D and Naef F 2014 *Mol. Syst. Biol.* **10** 739
[25] Paijmans J, Lubensky D K and ten Wolde P R 2017 *Phys. Rev.* E **95** 052403
[26] Dies M, Galera-Laporta L and Garcia-Ojalvo J 2016 *Integr. Biol.* **8** 533–41
[27] Harada T, Tanaka H A, Hankins M J and Kiss I Z 2010 *Phys. Rev. Lett.* **105** 088301
[28] Granada A E and Herzel H 2009 *PLoS One* **4** e7057
[29] Forger D B and Paydarfar D 2004 *J. Theor. Biol.* **230** 521–32
[30] Bagheri N, Stelling J and Doyle F J III 2008 *PLoS Comput. Biol.* **4** e1000104
[31] Page K M and Perez-Carrasco R 2018 *J. R. Soc. Interface* **15** 142
[32] Godin M *et al* 2010 *Nat. Methods* **7** 387–90
[33] Datseris A and Parlitz U 2022 *Nonlinear Dynamics: A Concise Introduction Interlaced with Code* (Berlin: Springer)
[34] Vind J, Sørensen M A, Rasmussen M D and Pedersen S 1993 *J. Mol. Biol.* **231** 678–88
[35] Klumpp S and Hwa T 2008 *Proc. Natl Acad. Sci. USA* **105** 20245–50
[36] Yang Q, Pando B F, Dong G, Golden S S and van Oudenaarden A 2010 *Science* **327** 1522–6
[37] Paijmans J, Bosman M, Ten Wolde P R and Lubensky D K 2016 *Proc. Natl Acad. Sci. USA* **113** 4063–8